Proton-air cross section measurement with the ARGO-YBJ cosmic ray experiment

G. Aielli,[1,2] C. Bacci,[3,4] B. Bartoli,[5,6] P. Bernardini,[7,8] X. J. Bi,[9] C. Bleve,[7,8] P. Branchini,[4] A. Budano,[4] S. Bussino,[3,4] A. K. Calabrese Melcarne,[10] P. Camarri,[1,2] Z. Cao,[9] A. Cappa,[11,12] R. Cardarelli,[2] S. Catalanotti,[6,5] C. Cattaneo,[13] P. Celio,[3,4] S. Z. Chen,[9] Y. Chen,[9] N. Cheng,[9] P. Creti,[8] S. W. Cui,[14] B. Z. Dai,[15] G. D'Alí Staiti,[16,17] Danzengluobu,[18] M. Dattoli,[11,12,19] I. De Mitri,[7,8,*] B. D'Ettorre Piazzoli,[6,5] M. De Vincenzi,[3,4] T. Di Girolamo,[6,5] X. H. Ding,[18] G. Di Sciascio,[2] C. F. Feng,[20] Zhaoyang Feng,[9] Zhenyong Feng,[21] F. Galeazzi,[4] P. Galeotti,[11,19] R. Gargana,[4] Q. B. Gou,[9] Y. Q. Guo,[9] H. H. He,[9] Haibing Hu,[18] Hongbo Hu,[9] Q. Huang,[21] M. Iacovacci,[6,5] R. Iuppa,[1,2] I. James,[3,4] H. Y. Jia,[21] Labaciren,[18] H. J. Li,[18] J. Y. Li,[20] X. X. Li,[9] B. Liberti,[2] G. Liguori,[13,22] C. Liu,[9] C. Q. Liu,[15] M. Y. Liu,[14] J. Liu,[15] H. Lu,[9] X. H. Ma,[9] G. Mancarella,[7,8] S. M. Mari,[3,4] G. Marsella,[8,23] D. Martello,[7,8] S. Mastroianni,[5] X. R. Meng,[18] P. Montini,[3,4] C. C. Ning,[18] A. Pagliaro,[24,16] M. Panareo,[8,23] L. Perrone,[8,23] P. Pistilli,[3,4] X. B. Qu,[20] E. Rossi,[5] F. Ruggieri,[4] L. Saggese,[6,5] P. Salvini,[13] R. Santonico,[1,2] P. R. Shen,[9] X. D. Sheng,[9] F. Shi,[9] C. Stanescu,[4] A. Surdo,[8] Y. H. Tan,[9] P. Vallania,[11,12] S. Vernetto,[11,12] C. Vigorito,[11,12] B. Wang,[9] H. Wang,[9] C. Y. Wu,[9] H. R. Wu,[9] B. Xu,[21] L. Xue,[20] Y. X. Yan,[14] Q. Y. Yang,[15] X. C. Yang,[15] A. F. Yuan,[18] M. Zha,[9] H. M. Zhang,[9] JiLong Zhang,[9] JianLi Zhang,[9] L. Zhang,[15] P. Zhang,[15] X. Y. Zhang,[20] Y. Zhang,[9] Zhaxisangzhu,[18] X. X. Zhou,[21] F. R. Zhu,[9] Q. Q. Zhu,[9] and G. Zizzi[7,8]

(The ARGO-YBJ Collaboration)

[1]*Dipartimento di Fisica dell'Università "Tor Vergata" - via della Ricerca Scientifica 1 - 00133 Roma - Italy*
[2]*Istituto Nazionale di Fisica Nucleare - Sezione di Tor Vergata - via della Ricerca Scientifica 1 - 00133 Roma - Italy*
[3]*Dipartimento di Fisica dell'Università "Roma Tre" - via della Vasca Navale 84 - 00146 Roma - Italy*
[4]*Istituto Nazionale di Fisica Nucleare - Sezione di Roma3 - via della Vasca Navale 84 - 00146 Roma - Italy*
[5]*Istituto Nazionale di Fisica Nucleare -*
Sezione di Napoli - Complesso Universitario di Monte Sant'Angelo - via Cintia - 80126 Napoli - Italy
[6]*Dipartimento di Fisica dell'Università di Napoli - Complesso Universitario di Monte Sant'Angelo - via Cintia - 80126 Napoli - Italy*
[7]*Dipartimento di Fisica dell'Università del Salento - via per Arnesano - 73100 Lecce - Italy*
[8]*Istituto Nazionale di Fisica Nucleare - Sezione di Lecce - via per Arnesano - 73100 Lecce - Italy*
[9]*Key Laboratory of Particle Astrophyics - Institute of High Energy Physics -*
Chinese Academy of Science - P.O. Box 918 - 100049 Beijing - P.R. China
[10]*Istituto Nazionale di Fisica Nucleare - CNAF - viale Berti-Pichat 6/2 - 40127 Bologna - Italy*
[11]*Istituto Nazionale di Fisica Nucleare - Sezione di Torino - via P. Giuria 1 - 10125 Torino - Italy*
[12]*Istituto di Fisica dello Spazio Interplanetario dell'Istituto Nazionale di Astrofisica - corso Fiume 4 - 10133 Torino - Italy*
[13]*Istituto Nazionale di Fisica Nucleare - Sezione di Pavia - via Bassi 6 - 27100 Pavia - Italy*
[14]*Hebei Normal University - Shijiazhuang 050016 - Hebei - China*
[15]*Yunnan University - 2 North Cuihu Rd - 650091 Kunming - Yunnan - P.R. China*
[16]*Istituto Nazionale di Fisica Nucleare - Sezione di Catania - Viale A. Doria 6 - 95125 Catania - Italy*
[17]*Università degli Studi di Palermo -*
Dipartimento di Fisica e Tecnologie Relative - Viale delle Scienze - Edificio 18 - 90128 Palermo - Italy
[18]*Tibet University - 850000 Lhasa - Xizang - P.R. China*
[19]*Dipartimento di Fisica Generale dell'Università di Torino - via P. Giuria 1 - 10125 Torino - Italy*
[20]*Shandong University - 250100 Jinan - Shandong - P.R. China*
[21]*South West Jiaotong University - 610031 Chengdu - Sichuan - P.R. China*
[22]*Dipartimento di Fisica Nucleare e Teorica dell'Università di Pavia - via Bassi 6 - 27100 Pavia - Italy*
[23]*Dipartimento di Ingegneria dell'Innovazione - Università del Salento - 73100 Lecce - Italy*
[24]*Istituto di Astrofisica Spaziale e Fisica Cosmica di Palermo -*
Istituto Nazionale di Astrofisica - via Ugo La Malfa 153 - 90146 Palermo - Italy

The proton-air cross section in the energy range 1–100 TeV has been measured by the ARGO-YBJ cosmic ray experiment. The analysis is based on the primary cosmic ray flux attenuation for different atmospheric depths (i.e. zenith angles) and exploits the detector capabilities of selecting the shower development stage by means of hit multiplicity, density and lateral profile measurements at ground. The effects of shower fluctuations, the contribution of heavier primaries and the uncertainties of the hadronic interaction models, have been taken into account. The results have been used to estimate the total proton-proton cross section at center-of-mass energies between 70 and 500 GeV, where no accelerator data are currently available.

*Corresponding author (ivan.demitri@le.infn.it)

I. INTRODUCTION

In the last decades, high-energy proton-antiproton colliders allowed extending the study of hadronic interactions up to center-of-mass energy $\sqrt{s} = 1.8$ TeV [1–3]. Moreover LHC experiments at CERN are expected to analyze proton-proton collisions and to measure total cross sections at $\sqrt{s} = 14$ TeV [4]. Anyway, at energies exceeding $\sqrt{s} \simeq 70$ GeV, total cross sections have not yet been measured at p-p machines and data from p-$\bar{p}$ colliders are still missing in the range 70 GeV $\lesssim \sqrt{s} \lesssim 500$ GeV [5,6].

The study of cosmic ray (CR) induced showers provides a unique opportunity to explore hadron interactions in an energy range which not only covers the LHC region, but also extends well beyond it, the natural beam of primary particles spanning up to extreme values [7]. Furthermore, some phase space regions cannot be easily accessed at colliders, where, as an example, most of the produced particles might escape undetected in the beam pipe in the case of *soft*, i.e. low momentum transfer, hadronic interactions. On the contrary, *soft* collisions play a major role in the development of CR-induced showers, carrying energy deep down in the atmosphere. In currently used interaction models, these collisions are treated by means of the Gribov-Regge Theory (GRT) [8] via *Pomerons* exchange [9], while a perturbative QCD approach can be appropriate at most collider experiments. Finally, it must be considered that, in the case of CR experiments, the collision targets are light nuclei (i.e. N, O, etc., hereafter ''*air*'' nuclei) and nuclear effects cannot be neglected. These aspects make somehow complementary the two approaches and cause their comparison to be extremely interesting from the point of view of very high-energy (astro)particle physics.

In CR experiments, the proton-air (hereafter p-air) cross section can be measured in several ways depending on the energy range and detection technique. Suitable models can then be used to estimate the p-p cross section [6]. Because of the rapidly falling CR energy spectrum, the use of ground based detectors is mandatory. This obviously implies that the method systematics are larger with respect to accelerator experiments, the interaction initial state being not under control. Moreover, as pointed out in [10], these experiments are actually sensitive only to the so-called *production* cross section defined as

$$\sigma_{p\text{-air}}^{\text{prod}} = \sigma_{p\text{-air}}^{\text{tot}} - \sigma_{p\text{-air}}^{\text{el}} - \sigma_{p\text{-air}}^{\text{qel}} \qquad (1)$$

where $\sigma_{p\text{-air}}^{\text{tot}}$ and $\sigma_{p\text{-air}}^{\text{el}}$ are the total and the elastic cross sections, respectively, while $\sigma_{p\text{-air}}^{\text{qel}}$ refers to quasielastic processes in which the nucleus gets excited without secondary particle production. There is some ambiguity in the literature, since the quantity $\sigma_{p\text{-air}}^{\text{prod}}$, as defined in Eq. (1), has also been referred to as *inelastic* or *absorption* cross section. Here we will follow the terminology introduced in

[10]. For the sake of simplicity, in the following we will refer to $\sigma_{p\text{-air}}^{\text{prod}}$ simply as the p-air cross section or $\sigma_{p\text{-air}}$.

The p-air cross section is measured by evaluating the absorption of the primary proton flux penetrating the atmosphere. In principle, the distribution of the atmospheric depth, X_0, of the first interaction point of CR protons could give a measurement of the interaction length $\lambda_{p\text{-air}}$ (and then the cross section $\sigma_{p\text{-air}}$) in a straightforward way. Unfortunately, this information cannot be currently accessed and indirect methods have to be used. Up to now three experimental approaches have been adopted, depending on the primary energy range and detection techniques. Their comprehensive description is out of the scope of this paper. Here we will shortly list them and we will then focus, in the following sections, on the technique adopted in this work.

The first method dates back to 1960s and actually estimates the flux of protons that reach the detection level without having yet interacted producing an hadronic shower (see [11–13] and references therein). This is made by measuring the flux of unaccompanied hadrons crossing high altitude calorimeters equipped with a suitable veto system. The flux is then compared with the measured primary cosmic ray flux at the top of the atmosphere. One of the intrinsic systematic errors of this approach comes from the uncertainty on the primary proton flux that is used in the estimate of the p-air cross section. By using this technique, one of the first evidences of the rising of the total p-p cross section with energy has been established [14]. The reduction of the proton flux prevents the adoption of this method at high energies, where the experiments must rely on the observed extensive air showers (EAS) initiated by CR primaries at the top of the atmosphere.

EAS arrays can evaluate the primary proton absorption in the atmosphere by measuring the shower rates at different zenith angles (i.e. atmospheric depths) once the shower development stage and energy are constrained by observations at ground (see [15–18] and references therein). The measured number of muons, N_μ, is generally used to evaluate the shower energy (and to select proton-initiated events), while the number of charged particles at the detection level, N_e, gives an estimate of the shower development stage. In this case an important role can be played by the shower-to-shower fluctuations, that might decrease the experimental capability of properly measuring the p-air cross section [19,20]. Since these effects depend on cosmic ray energy and mass composition, on detector capabilities and location, and on actual analysis procedures, the sensitivity of each experiment has to be checked with detailed simulations. This technique, traditionally known as the $N_e - N_\mu$ method, has a further source of systematic un-

certainty which comes from the appreciable model dependence of the predicted muon numbers [21,22].

At even larger energies, the shower longitudinal profile can be directly measured with the air fluorescence technique (and/or using the lateral distribution of Čerenkov light at ground). The atmospheric depth of the maximum shower development stage, X_{max}, gives information on the CR beam absorption, i.e. on the p-air cross section (see [17,23,24] and references therein). In this case, one of the largest systematics comes from the uncertainties on CR composition. This effect is also present in the previously mentioned approaches, but it becomes more and more important with increasing primary energy. In particular, the effect of CR primaries heavier than protons is negligible in the first approach, while it is small in the second one and a correction can be applied on the basis of CR composition measurements. At extremely high energies the CR composition is not sufficiently well known in order for that correction to be applied without introducing a sizeable systematic uncertainty.

Once the p-air cross section is measured, theoretical models can be used to give the total p-p cross section. This conversion is essentially based on the Glauber theory [25] and has been discussed in several works [6,10,12,26–30].

In this paper we will report on the measurement of the *production* cross section between 1–100 TeV CR protons and air nuclei with the ARGO-YBJ experiment (see Sec. II). The analysis is based on the CR flux attenuation for different atmospheric depths, i.e. zenith angles, and exploits the high detector accuracy in reconstructing the shower properties at ground. This allows a different approach with respect to the standard $N_e - N_\mu$ method used in EAS experiments that operate at larger energies and with lower shower front sampling capabilities. The results have also been used to estimate the total p-p cross section at center-of-mass energies between 70 and 500 GeV, where no accelerator data are currently available [5]. The adopted strategy is discussed in Sec. III, while details on data selection and analysis procedure are given in Sec. IV. Results are then given in Sec. V together with the discussion of the method systematics. Conclusions are reported in Sec. VI.

II. THE ARGO-YBJ EXPERIMENT

Cosmic ray physics in the 1–1000 TeV energy range and very high energy (VHE) γ-ray astronomy are the main scientific goals of the ARGO-YBJ experiment, a full coverage extensive air shower array resulting from a collaboration between Chinese and Italian institutions [31,32]. The detector is operating in the YBJ International Cosmic Ray Observatory, located in the village of Yangbajing, about 90 km north-west from Lhasa, in the Tibet region (People's Republic of China) at an altitude of 4300 m above sea level, corresponding to a vertical atmospheric depth of about 610 g/cm^2. The apparatus, extensively described in [31,32], is a single layer detector logically divided into 154 units called *clusters* (7.64 × 5.72 m^2) each made by 12 Resistive Plate Chambers (RPCs) operated in streamer mode (see Fig. 1). Each RPC (1.25 × 2.80 m^2) is read out by using 10 pads (62 × 56 cm^2), which are further divided into 8 strips (62 × 7 cm^2) providing a larger particle counting dynamic range [33]. The signals coming from all the strips of a given pad are sent to the same channel of a multihit TDC. The whole system, in smooth data taking from mid 2006, provides a single hit (pad) time resolution at the level of 1 ns, which allows a complete and detailed three-dimensional reconstruction of the shower front with unprecedented space-time resolution (see Fig. 2). In order to fully investigate transient phenomena with an even smaller energy threshold, an independent *scaler mode* acquisition system has also been put in operation [34]. Finally, a system for the RPC analog charge readout [35] from larger pads, each one covering half a chamber (the so-called *big pads*), is now being implemented. This will allow extending the detector operating range from about 100 TeV up to PeV energies.
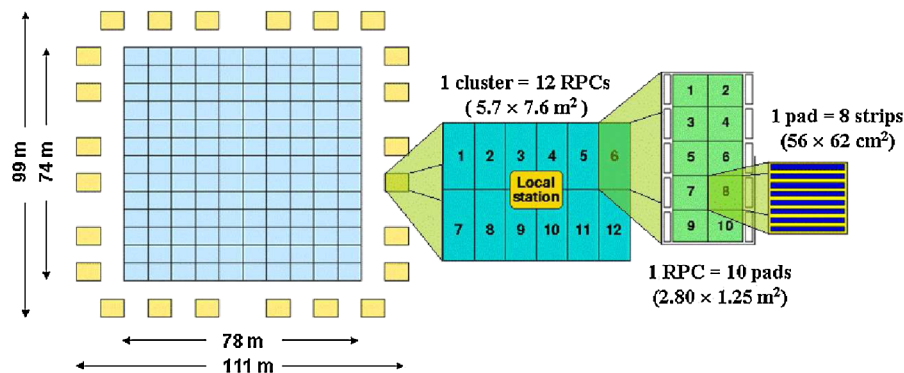

FIG. 1 (color online). The ARGO-YBJ detector setup. The *cluster* (12 RPCs) is the basic detector and DAQ unit equipped with a *Local Station* for its readout. The full-coverage central carpet is made by 130 clusters, the guard-ring by 24 clusters. The pad is the timing pixel and is further divided into 8 strips (see text).
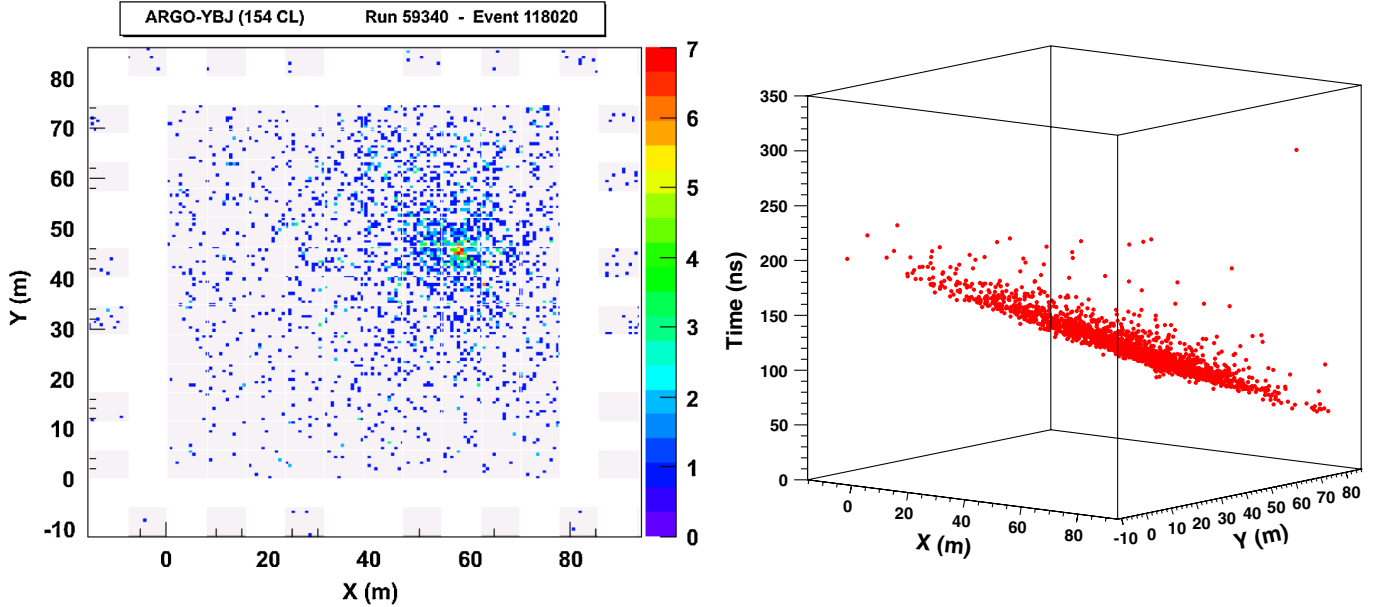
FIG. 2 (color online). Two different views of a detected shower. The hit map at ground is given on the left, the color code representing the strip multiplicity of each fired pad. A space-time view of the detected shower front is given on the right.

A suitable calibration procedure has been developed in order to remove systematic time offsets in the readout chain (due to front-end boards, TDC boards, cable lengths, etc.) among the 18480 different channels [36]. Many checks have been made in order to ensure the correctness of the procedure. One of these is made through the analysis of the position, size and shape of the reconstructed Moon and Sun shadows in the cosmic ray flux [37,38].

Because of the huge amount of data, event reconstruction is performed by using GRID-based object oriented technologies [39]. In the first event reconstruction step, the detected shower front is fitted to a plane. Actually, detailed simulations show that particles within several tens of meters from the shower core do form a curved front, which can be well approximated with a conical shape [40]. This is confirmed by experimental data and is suitably exploited in the second step of the event reconstruction. A reliable identification of the shower core position up to the edge, and slightly beyond, the active carpet is made through a Maximum Likelihood-based algorithm, using a NKG-like [41] lateral distribution function [42]. Space-time coordinates (positions and times of fired pads) are then fitted to a cone whose axis crosses the core position at ground [43]. As a result a very good angular resolution, σ_{ang} is obtained [38]. Obviously the actual value depends on the CR primary energy and mass (γ, p, He, …), and on the specific event selection criteria adopted in a given analysis. In our case, we get $\sigma_{\text{ang}}(E \sim 5 \text{ TeV}) \simeq 0.3°$ and $\sigma_{\text{ang}}(E \gtrsim 10 \text{ TeV}) \lesssim 0.2°$, for primary protons. This is particularly important, since it implies that no significant systematics are introduced by the detector angular resolution in the zenith angle distributions used for the cross section measurement (see Sec. V).

III. THE ANALYSIS STRATEGY

For a primary energy interval and for a given distance X_{dm} between the detector and the shower maximum (see Fig. 3), the frequency of showers as a function of zenith angle θ is directly related to the probability distribution of the depth of the shower maximum $P(X_{\text{max}})$, where $X_{\text{max}} = h_0 \sec\theta - X_{\text{dm}}$ and h_0 is the observation vertical depth. The shape of $P(X_{\text{max}} = X_0 + X_{\text{rise}})$ is given by the folding of the exponential dependence of the depth of the first interaction point X_0 (i.e. $e^{-X_0/\lambda_{p\text{-air}}}$ with $\lambda_{p\text{-air}}(\text{g/cm}^2) \simeq 2.41 \times 10^4/\sigma_{p\text{-air}}(\text{mb})$), with the probability distribution of X_{rise}, which includes the fluctuations of the shower development up to its maximum. Then the effects of the limited experimental resolution have to be also taken into account. For sufficiently large X_{max} values, $P(X_{\text{max}})$ tends to be a simple exponential with a characteristic length $\Lambda = k\lambda_{p\text{-air}}$, where k depends on hadronic interactions and on the shower development in the atmosphere and its fluctuations [6,22,44,45]. The actual value of k must be evaluated with a full Monte Carlo (MC) simulation and it depends on the experimental approach, the primary energy and the detector response. It might also depend on the features of the hadronic interaction model adopted in the simulation, this being a further source of systematic uncertainty. Anyway several studies showed that this dependence is generally small [6,18,45]. Finally, the contribution of cosmic rays heavier than protons has to be estimated and minimized in order to get an unbiased proton-air cross section measurement.

As discussed in Sec. I, experiments using the air fluorescence technique have direct access to $P(X_{\text{max}})$, while EAS detectors measuring the particles at ground might
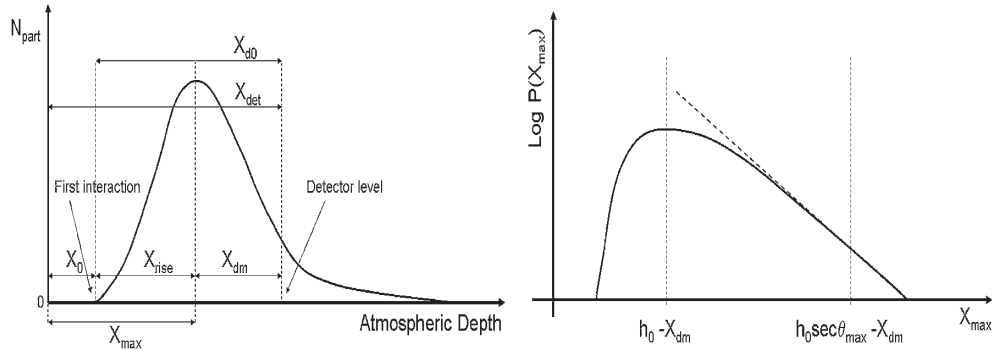
FIG. 3.   Simplified scheme of the shower longitudinal development in the atmosphere (left panel) and of the X_{max} distribution (right panel), together with the definitions of the quantities used in the text.

sample it through the flux dependence on zenith angle, once X_{dm} (or the shower age) has been fixed or constrained, within the limits of detector capabilities. In these cases the combination of CR energy, detector vertical depth, angular and X_{dm} ranges, actually define the part of the X_{max} distribution that can be accessed. A good performance is obtained if the exponential tail of $P(X_{\mathrm{max}})$ can be sampled. As it is schematically shown in Fig. 3, this requires selecting showers with the maximum development not far from the detection level (i.e. minimizing X_{dm}) and, obviously, exploring a zenith angle region as wide as possible.

If this is not the case, a flattening of the distribution might be observed, also due to shower fluctuations, resulting in a larger value of the parameter k and a lower sensitivity to $\sigma_{p\text{-air}}$. The measurement can be spoiled also by a very poor energy resolution. In this case both shower-to-shower fluctuations and the X_{rise} dependence on the primary energy might contribute to a worsening of the analysis performance. In some particular cases even the exponential behavior can be lost [22].

The ARGO-YBJ detector features and location (full coverage, angular resolution, fine granularity, small atmospheric depth, etc.), which ensure the capability of reconstructing the detected showers in a very detailed way, have been used to define the energy ranges and to constrain the shower ages. In particular, different hit (i.e. strip) multiplicity windows have been used to select showers corresponding to different primary energies, while the information on particle density, lateral profile and shower front extension has been used to constrain X_{dm} in the proper range. These features allowed the observation of the exponential falling of shower frequencies, through the secθ distribution.

The fit to the angular distribution $R(\theta)$ gives the slope value α, connected to the observed characteristic length Λ through the relation $\alpha = h_0/\Lambda$, being

$$R(\theta) = A(\theta)R_0 e^{-\alpha(\sec\theta - 1)}, \qquad (2)$$

where $R_0 = R(\theta = 0)$, and the factor $A(\theta)$ takes into account the geometrical acceptance of each angular bin.

The same analysis chain is then applied to the simulated data sample (see next section). For each strip multiplicity (i.e. primary energy) interval, the fit to the secθ distribution with the function of Eq. (2) gives the value of Λ^{MC}. The value of k, referring to each multiplicity bin, can then be evaluated as $k = \Lambda^{\mathrm{MC}}/\lambda^{\mathrm{MC}}_{p\text{-air}}$, where $\lambda^{\mathrm{MC}}_{p\text{-air}}$ is known, in the corresponding energy region, from the adopted interaction model.

The experimental interaction length is obtained by correcting the observed characteristic length $\Lambda^{\mathrm{exp}}_{\mathrm{CR\text{-}air}}$ by the factor k determined on the basis of the MC simulation: $\lambda^{\mathrm{exp}}_{\mathrm{CR\text{-}air}} = \Lambda^{\mathrm{exp}}_{\mathrm{CR\text{-}air}}/k$. Such value will give the measured p-air interaction length ($\lambda^{\mathrm{exp}}_{p\text{-air}}$), once the effects of heavier nuclei present in the primary cosmic ray flux have been taken into account. This has been made by evaluating the change of the slope α (see Eq. (2)) produced by the addition of the corresponding helium fraction to the proton primary flux in the MC simulation, the contribution of heavier nuclei being negligible.

The proton-air *production* cross section is then obtained from the previously mentioned relation: $\sigma_{p\text{-air}}(\mathrm{mb}) = 2.41 \times 10^4/\lambda^{\mathrm{exp}}_{p\text{-air}}(\mathrm{g/cm^2})$, while several theoretical models can be used to get the corresponding total proton-proton cross section $\sigma_{p\text{-}p}$ (see Sec. V).

IV. DATA SELECTION AND MONTE CARLO SIMULATION

The analysis was applied to a data sample of about 6.5×10^8 events collected by the central part of the detector, i.e. the 130 adjoining clusters fully covering a surface of 78×74 m^2 (see Fig. 1). An inclusive trigger requiring at least 20 fired pads in a 420 ns time window was used. In order to have both a small contamination of *external* events (i.e. those events with the true core position outside the carpet but reconstructed inside) and an angular resolution better than 0.5°, only events with at least 500 fired strips were considered. Moreover, the analysis was restricted to events with reconstructed zenith angle $\theta \leq 40°$. This was made in order to avoid effects due to the possible zenith angle

dependence of the analysis cuts, that might occur at $\theta \gtrsim 45°$ (see below).

A suitable simulation chain was also set up to check the effects of the different analysis cuts and to estimate possible systematics. About 10^8 proton-initiated and 2×10^7 He-initiated showers, with the corresponding power law energy spectra between 300 GeV and 3000 TeV and zenith angle up to 45°, were produced with the *CORSIKA* code [46]. In order to have a better evaluation of systematics, we produced independent samples by using three different hadronic interaction models: *QGSJET-I* [47], *QGSJET-II.03* [48], and *SIBYLL-2.1* [49,50]. As reference values for the energy spectral indexes and the p/He relative normalization we used those given in [51] and resulting from a global fit of existing experimental data. A full simulation of the detector response, based on the GEANT package [52], was performed, including also the effects of time resolution, trigger logic, electronics noise, etc. Simulated

data have been produced in the same format used for real ones and they have been analyzed by using the same reconstruction code. The reliability of the simulation procedure was successfully checked in several ways. As an example, in Fig. 4 there is a comparison between real data and the MC simulation, for two of the quantities used in the analysis. As can be seen, the agreement is good both before and after applying the adopted event selection cuts (see below). Moreover, as expected, the agreement gets worse if a pure proton composition is used for the CR primary flux in the MC sample.

In the analysis of real data, after a first selection based on the quality of the reconstruction procedure, a further rejection of *external* showers was performed with several additional cuts discussed in the following. The reconstructed core position, P_{rc}, was required to be in a fiducial area given by the inner 11×8 RPC clusters (corresponding to a total surface of about 64×64 m^2). This cut
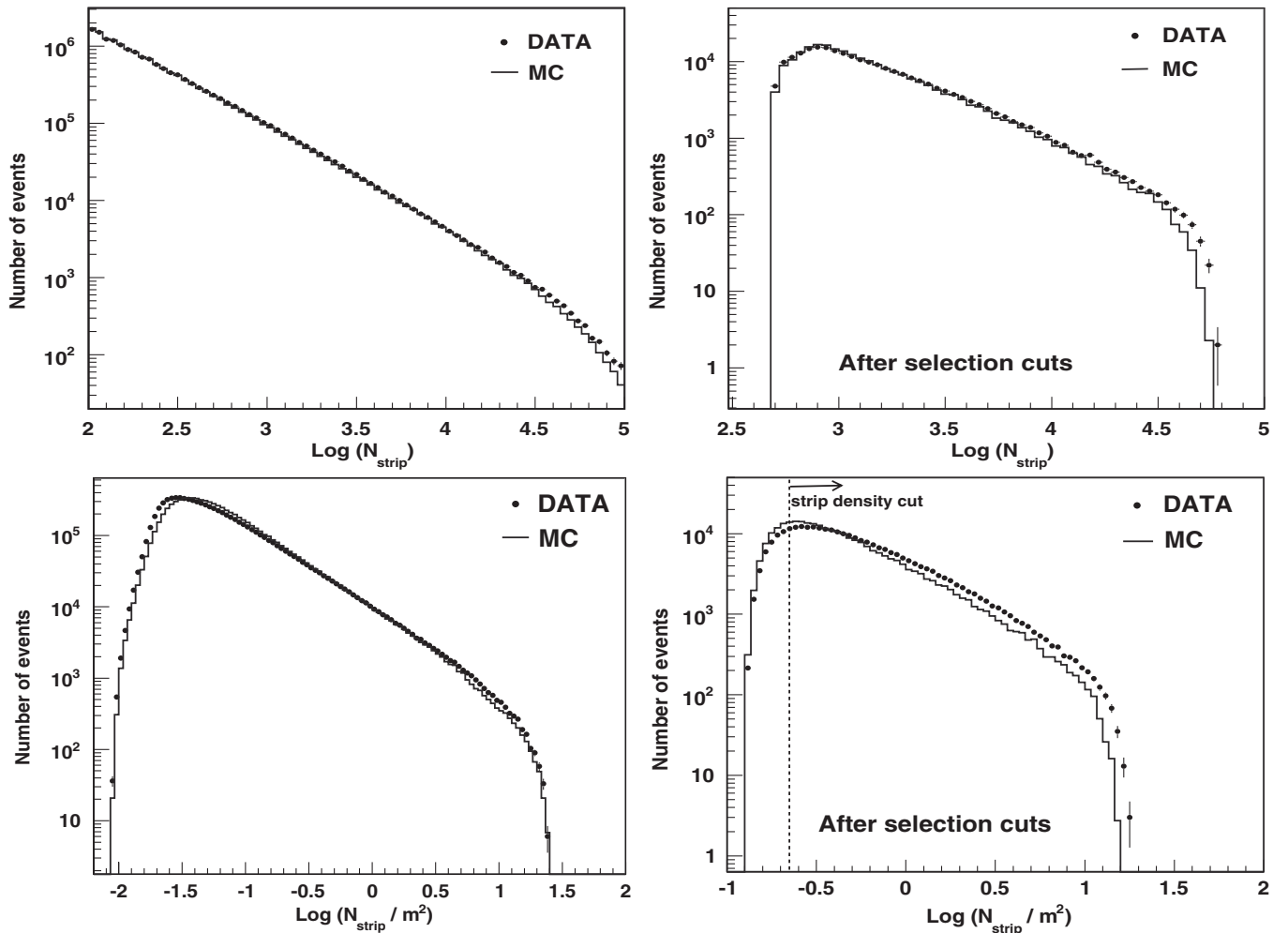

FIG. 4.   Comparison between simulated and real data before (left) and after (right) the application of selection cuts. The distributions of strip multiplicity are reported in the upper panels. In the lower ones the strip density near the shower core are shown, for events with the reconstructed core position inside the inner 11×8 RPC clusters (see text). The simulated sample include also helium initiated showers. As can be seen the agreement is good. Real and simulated distributions have been normalized, for comparison, to the same total number of events.
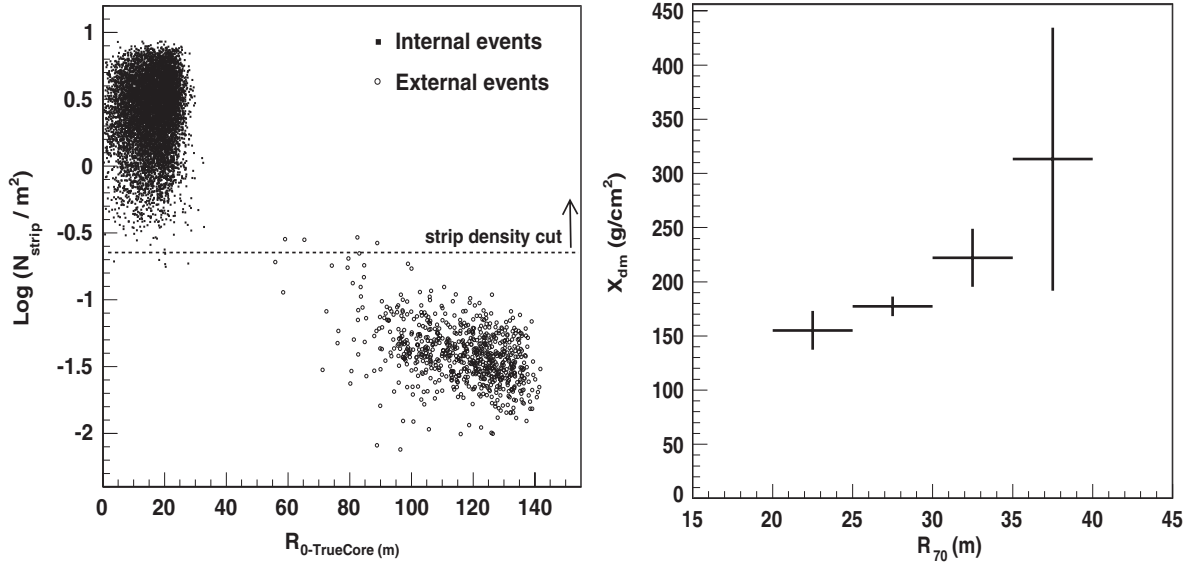
FIG. 5. Left panel: Correlation between the strip density near the reconstructed core and the distance of the true shower core from the detector center. As can be seen, the *density cut* (dashed line) is able to efficiently reject misreconstructed events. Right panel: Correlation between R_{70} and X_{dm}. The cut $R_{70} \leq 30$ m allows the selection of events with small X_{dm} (i.e. deeper shower maximum). These plots refer to simulated proton-induced showers processed as real data (see text).

reduced the initial data set to about 45% of the events with reconstructed $\theta \leq 40°$ and $N_{strip} \geq 500$. The quantity R_{70} was then introduced as the radius of the smallest circle (lying on the detector plane and centered in P_{rc}) containing 70% of the fired strips. It was then required that the distance of P_{rc} from the detector center plus R_{70} should be less than 50 m. The aim of this cut was to select showers largely contained inside the detector area (thus very well reconstructed). As a result, the data sample was reduced to $\sim$20% of the initial one. One further cut required the minimum average fired strip density, within a distance R_{70} from the reconstructed core, to be 0.2 strips/m^2 in the shower plane. Simulations indicate that this *density cut* allows the efficient rejection of *external* events, as shown in Fig. 5, left panel. The same purpose motivated the last selection cut (a *compactness cut*), requiring the R_{70} radius to be at most 30 m. Monte Carlo simulations show that this *compactness cut* is also related to the shower development stage, allowing the constraint of the value of X_{dm} (Fig. 5, right panel) and the selection of showers with their maximum lying deep in the atmosphere (i.e. the sampling of the exponential tail of the X_{max} distribution).

As already pointed out in Sec. III, this is an important point for the extraction of cross section data from the secθ distribution. The last two cuts finally selected 12% of the events reconstructed with $\theta \leq 40°$ and $N_{strip} \geq 500$ in the initial data sample. The fractions of events surviving each analysis cut were checked to be consistent with the corresponding quantities for MC data. Indeed, once the contribution of CR primaries heavier than protons were considered, all the values were in agreement and independent of the adopted hadronic interaction model.

The selected data sample was split into five different bins of strip multiplicity ΔN_{strip} (see Table I), starting from the threshold value of 500 fired strips on the whole central detector (out of the total 124800), in the trigger time window of 420 ns. As shown in Table I, each strip multiplicity bin corresponds to a different primary energy interval. In particular the averages of the Log(E) distributions are reported (after the application of all the selection criteria) together with their root mean square values. The energy values E assigned in this way were checked to be equivalently given by the median energies E_{50} of the corresponding event samples, and to be inde-

TABLE I. Strip multiplicity intervals, corresponding proton primary energies, and correction factors k with their statistical and systematic uncertainties (see text).

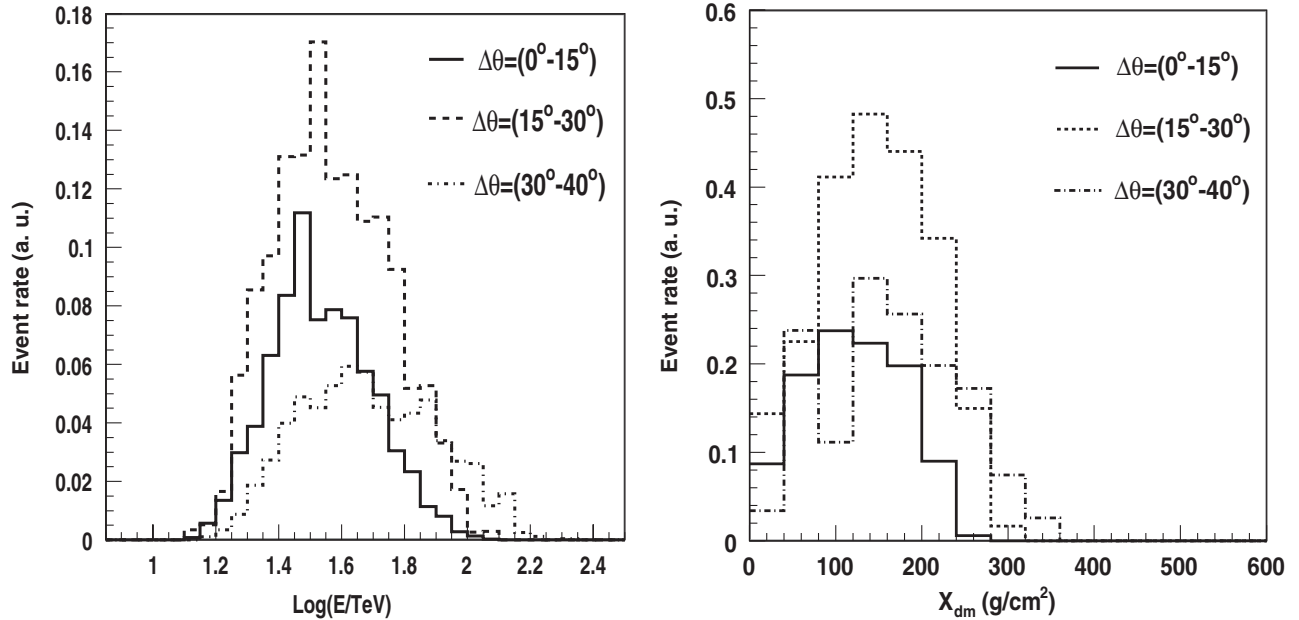| ΔN_{strip}	Log(E/eV)	$k_{QGSJET-I}$	$k_{QGSJET-II.03}$	$k_{SIBYLL-2.1}$	k
$500 \div 1000$	12.6 ± 0.3	$1.98 \pm 0.06 \pm 0.05$	$1.84 \pm 0.14 \pm 0.05$	$1.87 \pm 0.08 \pm 0.04$	$1.93 \pm 0.05 \pm 0.06$
$1500 \div 2000$	13.0 ± 0.2	$1.59 \pm 0.03 \pm 0.04$	$1.75 \pm 0.12 \pm 0.04$	$1.76 \pm 0.06 \pm 0.04$	$1.63 \pm 0.03 \pm 0.08$
$3000 \div 4000$	13.3 ± 0.2	$1.69 \pm 0.05 \pm 0.03$	$1.63 \pm 0.13 \pm 0.03$	$1.72 \pm 0.05 \pm 0.03$	$1.70 \pm 0.03 \pm 0.04$
$5000 \div 8000$	13.6 ± 0.2	$1.74 \pm 0.05 \pm 0.03$	$1.97 \pm 0.17 \pm 0.04$	$1.91 \pm 0.05 \pm 0.03$	$1.84 \pm 0.03 \pm 0.10$
>8000	13.9 ± 0.3	$2.04 \pm 0.06 \pm 0.05$	$2.23 \pm 0.19 \pm 0.05$	$2.01 \pm 0.05 \pm 0.05$	$2.03 \pm 0.04 \pm 0.10$

FIG. 6.   Energy and X_{dm} distributions (left and right panel, respectively) for proton-initiated MC events, corresponding to one of the strip multiplicity ranges, after the whole event selection procedure has been applied. As can be seen the effect of selection cuts does not introduce any substantial zenith-dependent bias.

pendent of the hadronic interaction model used in the simulation.

Simulations also show that, after applying all the analysis cuts, the contamination of *external* events misreconstructed as internal is less than 1% for all the energy bins.

In order to avoid any bias in the cross section measurement, a check has been made that the event selection was independent of the zenith angle. As an example, the distributions of primary energies and X_{dm} of simulated events surviving the analysis selection criteria are shown in Fig. 6, for different zenith angle intervals. The distributions are independent of the zenith angle up to about 40°, thus showing that the experimental sensitivity is not compromised by shower-to-shower fluctuations [19,20].

V. ANALYSIS RESULTS AND DISCUSSION

The result of the application of the whole selection procedure to real data is given in Fig. 7, where the experimental $\sec\theta$ distributions for the five strip multiplicity ranges are shown, after correction for the geometrical acceptance of each angular bin. They clearly show the expected exponential behavior, this being a further check that the detector capabilities and the adopted analysis cuts brought to a proper selection of events for the cross section measurement. A slight deviation is present, for the lowest energy sample only, at small $\sec\theta$ values (therefore not included in the fit). This is interpreted as due to the effect of shower fluctuations (see Sec. III), the shower maximum being more distant from the detector for these events. Indeed, for the lowest energy sample $\langle X_{max}\rangle \simeq 390$ g/cm^2, while $\langle X_{max}\rangle \simeq 450$ g/cm^2 for the other ones.

The angular distributions obtained from the MC simulations are very similar to those obtained with real data and the same considerations can be applied. From these plots, the values of Λ^{MC} are extracted by fitting them to an exponential function, with the slope parameter given by $\alpha = h_0^{MC}/\Lambda^{MC}$, where h_0^{MC} is the nominal atmospheric vertical depth used in the simulation (see below). Such values, once divided by the values of $\lambda_{p\text{-air}}^{MC}$, give the parameter k for the different energies. In particular, for each of the five selected data samples, the averages of the corresponding distributions of $\lambda_{p\text{-air}}^{MC}$ are taken, while their root mean square values have been used for the evaluation of the systematic errors.

As mentioned before, we produced three independent MC samples with different hadronic interaction models, namely *QGSJET-I*, *QGSJET-II.03*, and *SIBYLL-2.1*, that are widely used for the simulation of EAS and have been shown to provide a consistent description of their properties [53]. In the 1–100 TeV primary energy range, their predictions for $\sigma_{p\text{-air}}$ are quite similar, while there are larger differences for the estimates of the rate of diffraction processes and for the inelasticity of proton air interactions [53,54]. This last quantity essentially gives the fraction of energy available for particle production [55–57] and is particularly important for the longitudinal development of the shower in the atmosphere. Actually the two models that show the largest differences among them are *QGSJET-I* and *SIBYLL-2.1*, while *QGSJET-II.03* gives predictions closer to those of *SIBYLL-2.1* (see for instance [58]). In order to have a comprehensive and conservative estimate
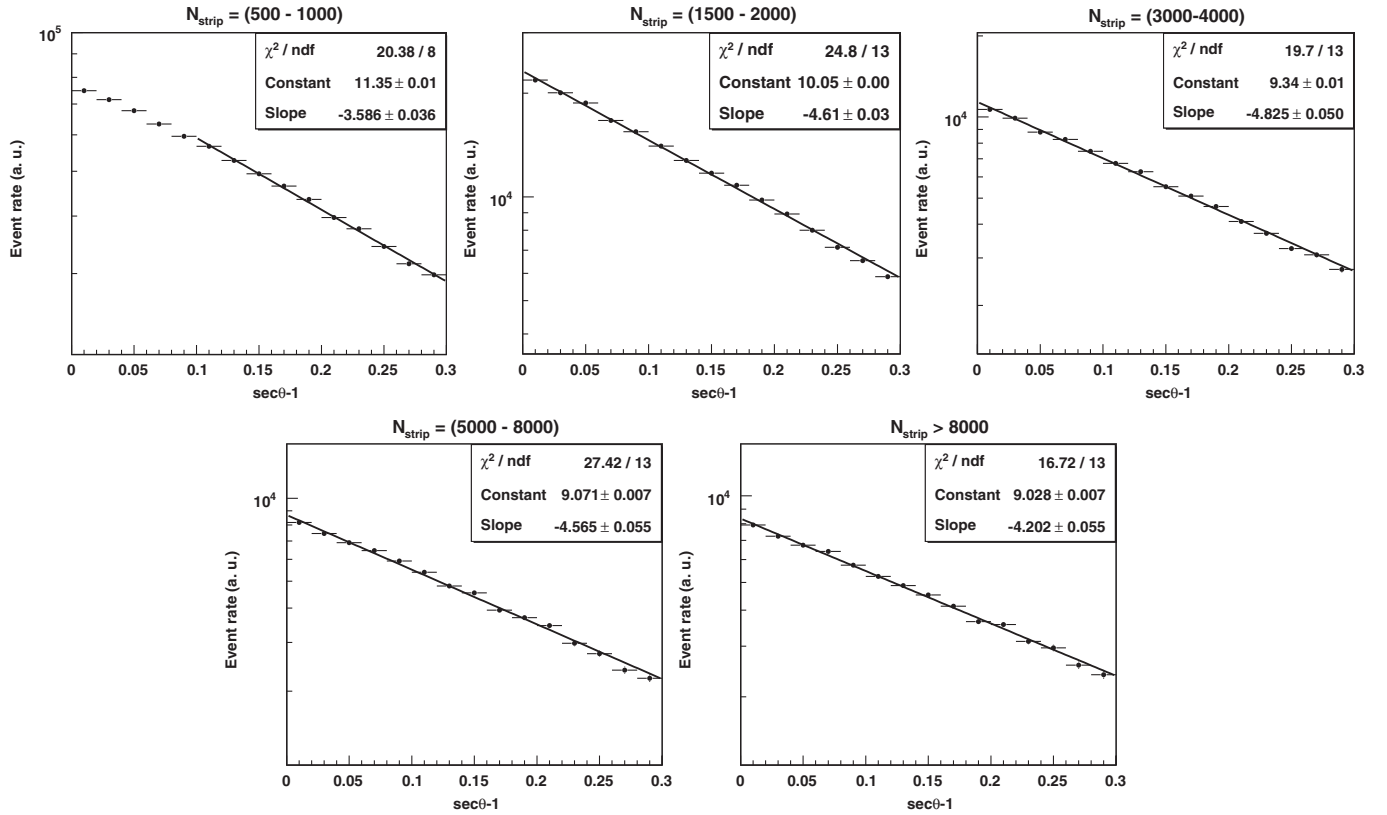
FIG. 7.   Experimental $\sec\theta$ distributions for the five strip multiplicity ranges, after correction for the geometrical acceptance in each angular bin.

of the systematic errors, we decided to consider all of them in the current analysis.

The factors k evaluated with *QGSJET-I*, *QGSJET-II.03* and *SIBYLL-2.1* are reported in Table I, where both the statistical and the systematic errors are also shown. The first ones come from the fit procedure, while the second ones from the root mean square values of the corresponding $\lambda_{p\text{-air}}^{\text{MC}}$ distributions. As can be seen, there is a general agreement, with larger differences between *QGSJET-I* and the other two models, as expected. These results are also consistent with the lower average inelasticity of *QGSJET-II.03* and *SIBYLL-2.1*, with respect to *QGSJET-I* in the considered energy range (see below). By following the just mentioned conservative approach, the results have then been combined to get the estimated k factors and the associated statistical and systematic errors (last column in Table I).

As already discussed in Sec. III, the value of k results from the contribution of many effects that are difficult to disentangle and depend on hadronic interactions, primary energy, shower-to-shower fluctuations, experiment location and capabilities, detection and analysis technique. As shown in [28,55], for ground array experiments a first contribution to k is given by:

$$k_0 \simeq \frac{1}{1 - \langle (1 - K_{\text{in}})^{\gamma - 1} \rangle} \tag{3}$$

where γ is the spectral index of the differential CR proton flux, K_{in} is the *p*-air inelasticity, and the symbol $\langle \ldots \rangle$ indicates averaging over events. At our energies the inelasticity is expected in the range $K_{\text{in}} \simeq 0.53 \div 0.60$ (depending on the assumed interaction model [54,59]), therefore implying $k_0 \simeq 1.25 \div 1.40$. Further contributions to k are expected from a flattening of the $\sec\theta$ distribution of selected events, produced by shower fluctuations and detector effects (see Sec. III), thus making k larger. This can be parametrized by a factor k_{det}, being $k = k_0 k_{\text{det}}$ [17,22].

As can be seen in Table I, in our case $k \simeq 1.6 \div 1.8$ (then we obtain $k_{\text{det}} \simeq 1.15 \div 1.45$), apart from the values obtained at the boundaries of the covered energy region. The larger value of k for the lowest energy bin is due to the smaller $\langle X_{\text{max}} \rangle$ value, that produces a larger effect of shower-to-shower fluctuations (see Sec. III). An explanation for the relatively high value of k in the highest energy bin is given by the onset of saturation of the strip digital information used in the analysis. This makes wider the energy interval actually contributing to the considered multiplicity bin, therefore implying a larger effect of fluctuations, mainly in terms of X_{rise}, with a consequent loss of sensitivity. These two effects practically define the energy region in which the current analysis can be performed. Important improvements will be achieved with the use of the analog RPC readout (see Sec. II).

A check was also made to verify that the detector angular resolution (see Sec. II) is sufficiently good in order not to introduce any bias in the cross section measurement. Indeed the slopes α obtained by using the true zenith angles θ or the reconstructed ones were in complete agreement, within the quoted errors, for all the five strip multiplicity MC samples.

In the simulations the vertical profile of Linsley's *standard atmosphere* was used [46] with the detection level set at the altitude of 4300 m a.s.l., corresponding to $h_0^{\mathrm{MC}} = 606.7$ g/cm^2. A small source of uncertainty in the p-air cross section measurement (see Eq. (2)) might be given by a systematic difference between h_0^{MC} and h_0 together with its variations with time due to the change of atmospheric conditions. From the pressure data continuously taken at Yangbajing, we evaluated $h_0^{\mathrm{MC}}/h_0 = 0.988 \pm 0.007$, resulting in an impact on the cross section analysis at the level of 1%, which has then been taken into account for the cross section data presented here.

As outlined in Sec. III, the measured $\Lambda_{\mathrm{CR\text{-}air}}^{\mathrm{exp}}$ value together with the k factor determined from the simulation, directly gives the experimental interaction length $\lambda_{\mathrm{CR\text{-}air}}^{\mathrm{exp}}$ and consequently the production cross section $\sigma_{\mathrm{CR\text{-}air}}$. At this stage, the cross section has still to be corrected for the contribution of CR primaries heavier than protons. This correction has been estimated by evaluating the effect of the introduction of helium primaries in the simulated data on the shape of the secθ distribution. Corrections for other primaries (i.e. CNO group, Fe, etc.) are negligible. Both the different absolute values and the energy dependences of proton and helium fluxes were considered, by taking as a reference the fits to the experimental data given in [51]. As expected, the simulations showed a slight steepening of the secθ distribution at the highest strip multiplicity intervals, thus changing the values of the corresponding cross section estimates. By applying this procedure we got the correction factors η to be applied to $\sigma_{\mathrm{CR\text{-}air}}$ in order to obtain $\sigma_{p\text{-air}}$ (see Table II). It has also been checked that the effect of primary particles heavier than protons on the shape of the secθ distribution, is limited to few per cent not only due to the CR beam composition itself, but also because the analysis cuts actually select a proton-enriched sample.

Indeed, the initial fraction of He-induced showers is further reduced by about a factor 1.9, through the analysis flow, with respect to proton-induced events.

The effect of the uncertainty of the primary CR composition has been estimated by applying the same procedure starting from other primary flux measurements, namely, those from the JACEE [60] and RUNJOB [61] experiments. We found small differences (below 4%) which were used for the evaluation of the systematic uncertainty on the factor η (see Table II).

The resulting proton-air production cross sections, $\sigma_{p\text{-air}}$, are summarized in Table II, where both statistical and systematic errors are reported. These results are consistent with a previous ARGO-YBJ measurement done without using the strip information [62], and also with a preliminary estimate obtained from the analysis of a data set taken with only 42 RPC clusters during the detector installation [63,64].

The measured p-air *production* cross section is reported, in Fig. 8, as a function of the primary proton energy. The results found by other experiments and the expectations given by some hadronic interaction models are also shown [46,65–67]. Even if data are in general agreement, it can be noticed some discrepancy between the various experimental approaches that might be due to the different method systematics (see Sec. I). Furthermore, new results, namely, those from ARGO-YBJ, TienShan [68], EAS-TOP [18] and HiRes [24], systematically give cross section values that are slightly lower with respect to the more recent and comprehensive hadronic interaction models actually used in these analyses. The indication for lower cross section (and/or inelasticity) values is also consistent with what found from the analysis of several other EAS observables [69–72]. Indeed, as previously pointed out, the inelasticity distribution in p-air interactions plays an important role in the longitudinal development of atmospheric showers. In EAS-based cross section measurements these effects are taken into account by the k factors. Anyway residual systematic differences between data and expectations at the level of few per cent might result from the modeling and the effect of very low inelasticity collisions (i.e. $K_{in} \lesssim 0.05$) that cannot actually be observed, being due to diffractive interactions that weakly (or do not) influence the EAS development [54,65,66], while are included in the cross section values given by the hadronic models in Fig. 8 [46,59]. This kind of effects might be different in the case of cross section evaluations based on measurements of the single hadrons flux at ground [11–13]. The low energy threshold of ARGO-YBJ (with respect to other EAS experiments) allows a direct comparison with the values given by this technique, showing a good agreement. This is particularly important since the systematics of the two measurement techniques are completely different. The agreement also extends to the predictions of different calculations based on the Glauber theory [25], applied to

TABLE II. Strip multiplicity intervals, correction factors for the helium contribution η, and proton-air cross sections thus obtained. The values of the resulting total proton-proton cross sections estimates are also reported. The errors given first come from statistics, the second ones from the systematics.

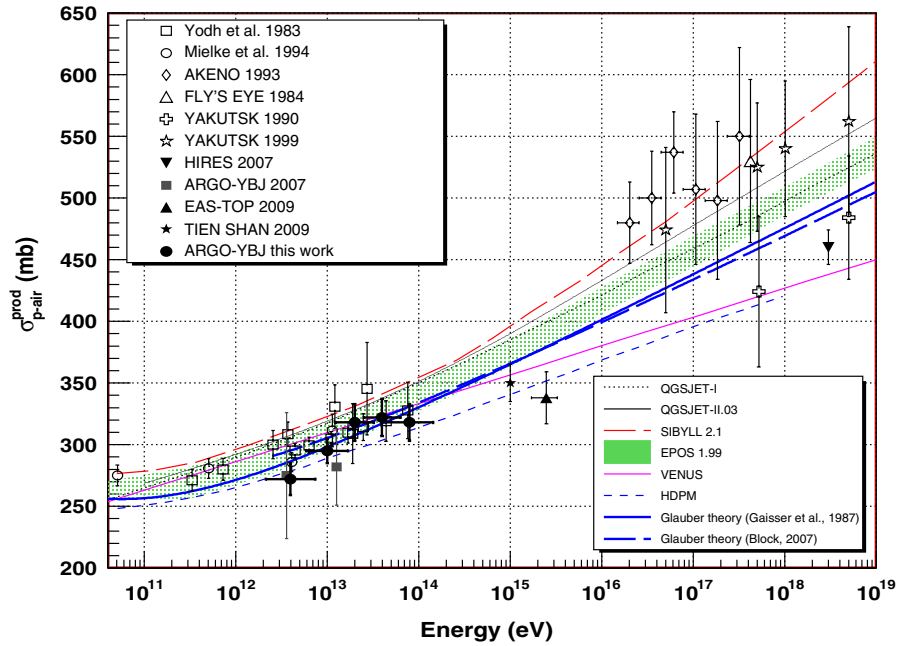| $\Delta N_{\mathrm{strip}}$	η	$\sigma_{p\text{-air}}$ (mb)	$\sigma_{p\text{-}p}$ (mb)
$500 \div 1000$	$1.00 \pm 0.04 \pm 0.01$	$272 \pm 13 \pm 9$	$43 \pm 3 \pm 5$
$1500 \div 2000$	$1.00 \pm 0.03 \pm 0.01$	$295 \pm 10 \pm 14$	$48 \pm 3 \pm 6$
$3000 \div 4000$	$0.99 \pm 0.04 \pm 0.01$	$318 \pm 15 \pm 8$	$54 \pm 4 \pm 6$
$5000 \div 8000$	$0.98 \pm 0.04 \pm 0.03$	$322 \pm 15 \pm 20$	$56 \pm 4 \pm 7$
>8000	$0.95 \pm 0.04 \pm 0.04$	$318 \pm 15 \pm 21$	$54 \pm 4 \pm 8$

FIG. 8 (color online). Proton-air *production* cross section measured by ARGO-YBJ and by other CR experiments [11–13,16–18,23,24,62,68] together with the values given by several hadronic interaction models [46,65–67]. Also shown are the predictions of two different calculations based on Glauber theory [12,30] applied to accelerator data as parametrized in [73]. In this plot ARGO-YBJ points have been already corrected for the effects of CR primaries heavier than protons.
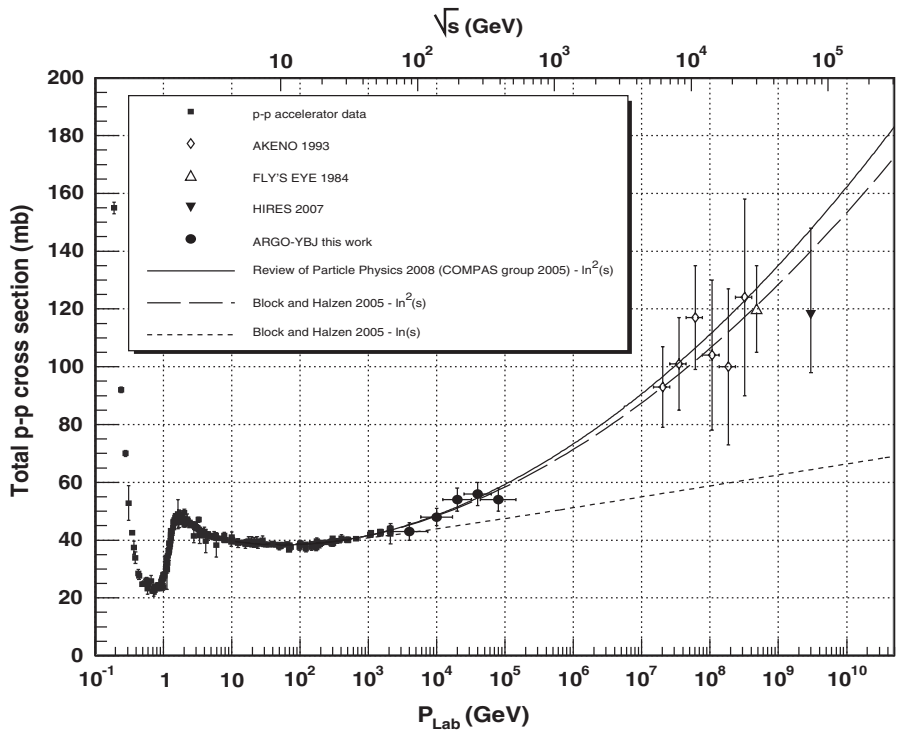

FIG. 9. Total *p-p* cross section, σ_{p-p}, obtained by ARGO-YBJ starting from $\sigma_{p\text{-air}}$ together with the same quantity published by other CR experiments [16,23,24]. The values of the total *p-p* cross section measured at accelerator experiments [5] are also reported. The lines result from a global analysis of accelerator data [5,73,75], assuming an asymptotic behavior of hadronic cross sections proportional to $\ln^2(s)$ or $\ln(s)$, as reported in the plot.

the measurements made at particle accelerators. As an example, the results of two of them [12,30] are actually shown in Fig. 8, starting from the accelerator data analysis performed in [73], where an asymptotic $\ln^2(s)$ dependence of hadronic cross sections is shown to be favored.

As outlined in Sec. I, Glauber theory can also be used to estimate the total proton-proton cross section $\sigma_{p\text{-}p}$, at energies not covered by accelerator data, by starting from the *p*-air *production* cross section $\sigma_{p\text{-air}}$ as measured by CR experiments. These calculations were discussed in several papers [6,10,12,26–30]. As pointed out by many authors [6], an essential step in the conversion is the knowledge of the dependence of the slope, B, of the forward scattering amplitude for elastic *p*-*p* collisions on the center-of-mass energy $\sqrt{s}$, or on $\sigma_{p\text{-}p}$ itself. For ARGO-YBJ data, we applied the conversion given in [12], that uses the somewhat model-independent Chou-Yang prescription [74] between B and the total cross section $\sigma_{p\text{-}p}$, this being also consistent with available measurements on $B(s)$. The results were compared with other models [26–30], the larger differences being with [28,29], that foresee slightly higher or lower $\sigma_{p\text{-}p}$ values, respectively. Anyway in all the cases the differences, in our energy range, are below 10% and they have been added as a further contribution to the systematic error on the resulting $\sigma_{p\text{-}p}$. The results are summarized in Table II and in Fig. 9. Also shown in the figure are the measurements performed at *p*-*p* accelerators [5] and the $\sigma_{p\text{-}p}$ values published by other CR experiments [16,23,24] starting from $\sigma_{p\text{-air}}$. As can be seen, the ARGO-YBJ data lie in an energy region not yet reached by *p*-*p* colliders and still lacking in *p*-$\bar{p}$ total cross section measurements. Our result is in agreement with the general trend of accelerator data showing the rise of the cross section with energy. In particular, it favors the asymptotic $\ln^2(s)$ increase of total hadronic cross sections as obtained in [73] from a global analysis of accelerator data.

VI. CONCLUSIONS

The study of CR-induced showers provides a unique opportunity to explore hadron interactions in energy ranges and phase space regions currently not accessible at particle colliders. In this paper, the cosmic ray flux attenuation for different atmospheric depths (i.e. zenith angles) has been exploited in order to measure the proton-air cross section in a laboratory energy range between approximately 1 TeV and 100 TeV, with the ARGO-YBJ experiment. The information provided by a highly segmented full coverage detector, allowed the introduction of selection cuts able to both define the energy scale and constrain the shower

development stage. The analysis results have been also used to estimate the total proton-proton cross section at center-of-mass energies between 70 and 500 GeV.

The analysis was applied to a data sample of about 6.5×10^8 events. A full simulation of the primary interaction, the shower development in the atmosphere, the particle detection at ground and the complete analysis procedure has also been setup and used in order to make consistency checks and evaluate the method systematics. The effects of shower fluctuations and the contribution of heavier primaries have been also considered. Moreover the use, in the simulations, of three different hadronic interaction models allowed a comprehensive and conservative estimate of the associated systematic uncertainties.

The results for the proton-air *production* cross section have been compared with previous measurements and model predictions. A good agreement is present with other measurements made in the same energy region with completely different techniques, and also with theoretical predictions based on particle accelerator data. Some systematic differences between more recent results and the values given by commonly adopted hadronic interaction models are present at the level of few per cent, the measured cross sections suggesting lower values and/or deeper shower development in the atmosphere.

The total proton-proton cross section $\sigma_{p\text{-}p}$ has then been inferred from the measured proton-air *production* cross section $\sigma_{p\text{-air}}$ by using the Glauber theory. The resulting data lie in an energy region not yet reached by *p*-*p* colliders and so far lacking in *p*-$\bar{p}$ total cross section measurements [1–3]. Our result is consistent with the general trend of experimental data, favoring an asymptotic $\ln^2(s)$ rise of the cross section.

Further improvements in the analysis are expected from the use of the detailed information on the shower front (curvature, rise time, time width, etc.) that ARGO-YBJ is able to record with very high precision, and by the implementation of the analog RPC readout that will allow extending these studies to collisions with center-of-mass energies up to the TeV region.

[1] C. Geich-Gimbel, Int. J. Mod. Phys. A **4**, 1527 (1989).
[2] C. Avila *et al.*, Phys. Lett. B **537**, 41 (2002).
[3] F. Abe *et al.*, Phys. Rev. D **50**, 5550 (1994).
[4] K. Österberg *et al.*, J. Phys. Conf. Ser. **110**, 022037 (2008); M. Deile *et al.*, arXiv:hep-ex/0602021.
[5] C. Amsler *et al.* (Particle Data Group), Phys. Lett. B **667**, 1 (2008).
[6] M. M. Block, Phys. Rep. **436**, 71 (2006), and references therein.
[7] J. Abraham *et al.*, Phys. Rev. Lett. **101**, 061101 (2008).
[8] L. V. Gribov *et al.*, Phys. Rep. **100**, 1 (1983).
[9] K. Werner, Phys. Rep. **232**, 87 (1993).
[10] R. Engel *et al.*, Phys. Rev. D **58**, 014019 (1998).
[11] G. B. Yodh *et al.*, Phys. Rev. D **27**, 1183 (1983).
[12] T. K. Gaisser *et al.*, Phys. Rev. D **36**, 1350 (1987).
[13] H. H. Mielke *et al.*, J. Phys. G **20**, 637 (1994).
[14] G. B. Yodh *et al.*, Phys. Rev. Lett. **28**, 1005 (1972).
[15] T. Hara *et al.*, Phys. Rev. Lett. **50**, 2058 (1983).
[16] M. Honda *et al.*, Phys. Rev. Lett. **70**, 525 (1993).
[17] S. P. Knurenko *et al.*, in *Proceedings of the 26th International Cosmic Ray Conference (ICRC99), Salt Lake City, Utah, (1999)*, (AIP), New York, 1999), Vol. 1, p. 372; M. N. Dyakonov *et al.*, in *Proceedings of the 21th International Cosmic Ray Conference (ICRC1990) Adelaide, Australia, HE. 3.7-8 (1990)*, (University of Adelaide), Adelaide, 1990), p. 252.
[18] M. Aglietta *et al.*, Phys. Rev. D **79**, 032004 (2009).
[19] J. Alvarez-Muñiz *et al.*, Phys. Rev. D **66**, 123004 (2002).
[20] J. Alvarez-Muñiz *et al.*, Phys. Rev. D **69**, 103003 (2004).
[21] T. Pierog and K. Werner, Phys. Rev. Lett. **101**, 171101 (2008).
[22] R. Ulrich *et al.*, New J. Phys. **11**, 065018 (2009), and references therein.
[23] R. M. Baltrusaitis *et al.*, Phys. Rev. Lett. **52**, 1380 (1984).
[24] K. Belov *et al.*, *Proceedings of the 30th International Cosmic Ray Conference (ICRC 07) (Universidad Nacional Autonoma de Mexico, Mexico City, Mexico, 2008)*, ID 1216 Vol. 4 (HE part 1), pp. 687–690.
[25] R. J. Glauber, in *Lectures in Theoretical Physics*, edited by W. E. Brittin and L. G. Dunham (Interscience, New York 1959), Vol. 1, p. 315; R. J. Glauber and G. Matthiae, Nucl. Phys. **B21**, 135 (1970).
[26] L. Durand and H. Pi, Nucl. Phys. B, Proc. Suppl. **12**, 379 (1990).
[27] B. Z. Kopeliovich *et al.*, Phys. Rev. D **39**, 769 (1989).
[28] J. Bellandi *et al.*, Phys. Lett. B **343**, 410 (1995).
[29] T. Wibig and D. Sobczynska, J. Phys. G **24**, 2037 (1998).
[30] M. M. Block, Phys. Rev. D **76**, 111503(R) (2007).
[31] C. Bacci *et al.*, Astropart. Phys. **17**, 151 (2002), and references therein.
[32] I. De Mitri *et al.*, Nucl. Phys. B, Proc. Suppl. **165**, 66 (2007).
[33] G. Aielli *et al.*, Nucl. Instrum. Methods Phys. Res., Sect. A **562**, 92 (2006).
[34] G. Aielli *et al.*, Astropart. Phys. **30**, 85 (2008).
[35] P. Creti *et al.*, *Proceedings of the 29th International Cosmic Ray Conference (ICRC 05), Pune, India* (Tata Institute of Fundamental Research), Mumbai, India, 2005), Vol. 8, p. 97.
[36] G. Aielli *et al.*, Astropart. Phys. **30**, 287 (2009); H. H. He *et al.*, Astropart. Phys. **27**, 528 (2007).
[37] G. D'Alì Staiti *et al.*, Nucl. Instrum. Methods Phys. Res., Sect. A **588**, 7 (2008).
[38] G. Di Sciascio *et al.*, *Proceedings of the Vulcano08 Workshop on Frontier Objects in Astrophysics and Particle Physics, Vulcano, Italy (2008)* (Societá Italiana di Fisica), Vulcano, Italy, 2008). , Also arXiv:0811.0997.
[39] C. Stanescu *et al.*, *Proceedings of the 30th International Cosmic Ray Conference (ICRC 07), Mexico City, Mexico 2008*, Universidad Nacional Autonoma de Mexico), Mexico City, 2008, ID 887, Vol. 5 (HE part 2), pp. 1057–1060, and references therein.
[40] A. K. Calabrese Melcarne *et al.*, *Proceedings of the 30th International Cosmic Ray Conference (ICRC 07) Mexico City, Mexico 2008*, (Universidad Nacional Autonoma de Mexico), Mexico City, 2008, ID 1100, Vol. 4 (HE part 1), pp. 139–142.
[41] K. Greisen, Annu. Rev. Nucl. Sci. **10**, 63 (1960); K. Kamata and J. Nishimura, Prog. Theor. Phys. Suppl. **6**, 93 (1958).
[42] G. Di Sciascio *et al.*, *Proceedings of the 28th International Cosmic Ray Conference (ICRC 03), Tsukuba, Japan*, (Universal Academy Press, Inc.), Tokyo, Japan, Session OG.2.5 (2003) p. 3015; D. Martello *et al.*, *Proceedings of the 27th International Cosmic Ray Conference (ICRC 01), Hamburg, Germany*, (Copernicus Gesellschaft), (2001), Vol. 7, p. 2927.
[43] D. Martello *et al.*, *Proceedings of the 28th International Cosmic Ray Conference (ICRC 03), Tsukuba, Japan*, (Universal Academy Press, Inc.), Tokyo, Japan, Session OG.2.5 (2003), p. 3011.
[44] R. W. Ellsworth *et al.*, Phys. Rev. D **26**, 336 (1982).
[45] C. L. Pryke, Astropart. Phys. **14**, 319 (2001).
[46] D. Heck *et al.*, *CORSIKA: A Monte Carlo Code to Simulate Extensive Air Showers (Forshungszentrum Karlsruhe, FZKA 6019, 1998)*, and references therein.
[47] N. N. Kalmykov *et al.*, Nucl. Phys. B, Proc. Suppl. **52** (1997).
[48] S. Ostapchenko, Nucl. Phys. B, Proc. Suppl. **151**, 143 (2006).
[49] R. Engel *et al.*, *Proceedings of the 26th International Cosmic Ray Conference (ICRC99), Salt Lake City, USA (1999)*, Vol. 1, p. 415.
[50] R. S. Fletcher *et al.*, Phys. Rev. D **50**, 5710 (1994).
[51] J. R. Hörandel, Astropart. Phys. **19**, 193 (2003).
[52] GEANT—Detector Description and Simulation Tool, CERN Program Library, Long Writeup, W5013, 1993.
[53] S. Ostapchenko, Nucl. Phys. B, Proc. Suppl. **175**, 73 (2008).
[54] R. Luna *et al.*, Phys. Rev. D **70**, 114034 (2004).
[55] Yu. M. Shabelski *et al.*, J. Phys. G **18**, 1281 (1992).
[56] T. K. Gaisser *et al.*, Phys. Rev. D **47**, 1919 (1993).
[57] G. M. Frichter *et al.*, Phys. Rev. D **56**, 3135 (1997).
[58] M. T. Dova and S. Ferrari, Eur. Phys. J. C **52**, 673 (2007).
[59] J. Alvarez-Muñiz *et al.*, Phys. Rev. D **66**, 033011 (2002).
[60] K. Asakimori *et al.*, Astrophys. J. **502**, 278 (1998).
[61] A. V. Apanasenko *et al.*, Astropart. Phys. **16**, 13 (2001).
[62] I. De Mitri *et al.*, *Proceedings of the 30th International Cosmic Ray Conference (ICRC07) (Universidad Nacional Autonoma de Mexico, Mexico City, Mexico, 2008)*, (Universidad Nacional Autonoma de Mexico), Mexico City, 2008, ID 950, Vol. 4 (HE part 1), pp. 675–678.

[63] M. Iacovacci *et al.*, Nucl. Phys. B, Proc. Suppl. **175**, 389 (2008).

[64] A. Surdo *et al.*, *Proceedings of the 20th European Cosmic Ray Symposium, Lisbon, Portugal, 2006.*

[65] J. Knapp *et al.*, Astropart. Phys. **19**, 77 (2003), and references therein.

[66] R. Ulrich *et al.*, *Proceedings of the 30th International Cosmic Ray Conference (ICRC 07) (Universidad Nacional Autonoma de Mexico, Mexico City, Mexico, 2008)*, (Universidad Nacional Autonoma de Mexico), Mexico City, 2008, ID 1027, Vol. 4 (HE part 1), pp. 679–682; arXiv:astro-ph/0706.2086v1, and references therein.

[67] T. Pierog and K. Werner, *Proceedings of the 31th International Cosmic Ray Conference (ICRC 09), Łódź, Poland, No. 428 (2009)*, (University of Łódź), Łódź,

Poland, (2009).

[68] A. P. Chubenko *et al.*, *Proceedings of the 31th International Cosmic Ray Conference (ICRC 09), Łódź, Poland, No. 222 (2009)*, (University of Łódź), Łódź, Poland, (2009).

[69] J. R. Hörandel, J. Phys. G **29**, 2439 (2003).

[70] A. D. Erlykin, Astropart. Phys. **27**, 521 (2007).

[71] J. Abdallah *et al.*, Astropart. Phys. **28**, 273 (2007).

[72] J. R. Hörandel *et al.*, *Proceedings of the 31th International Cosmic Ray Conference (ICRC 09), Łódź, Poland, No. 227 (2009)*, (University of Łódź), Łódź, Poland, (2009).

[73] M. M. Block and F. Halzen, Phys. Rev. D **72**, 036006 (2005).

[74] T. T. Chou and C. N. Yang, Phys. Lett. B **128**, 457 (1983).

[75] J. R. Cudell *et al.*, Phys. Rev. Lett. **89**, 201801 (2002).